Novel Battery-Less Wireless Sensors for Traffic Flow Measurement

Final Report

Prepared by:

Krishna Vijayaraghavan
Rajesh Rajamani

Department of Mechanical Engineering
University of Minnesota

CTS 08-16

Technical Report Documentation Page

1. Report No.	2.	3. Recipients Accession No.	
CTS 08-16			
4. Title and Subtitle Novel Battery-Less Wireless Sensors for Traffic Flow Measurement		5. Report Date November 2008 6.	
7. Author(s) Krishna Vijayaraghavan and Rajesh Rajamani		8. Performing Organization Report No.	
9. Performing Organization Name and Address Department of Mechanical Engineering University of Minnesota 1100 Mechanical Engineering 111 Church Street S.E. Minneapolis, Minnesota 55455		10. Project/Task/Work Unit No. CTS project # 2007047 11. Contract (C) or Grant (G) No.	
12. Sponsoring Organization Name and Address Intelligent Transportation Systems Institute University of Minnesota 200 Transportation and Safety Building 511 Washington Ave. SE Minneapolis, Minnesota 55455		13. Type of Report and Period Covered Final Report 14. Sponsoring Agency Code	
15. Supplementary Notes http://www.cts.umn.edu/Publications/ResearchReports/			

16. Abstract (Limit: 200 words)

This project presents a novel battery-less wireless sensor that can be embedded in the road and used to measure traffic flow rate, speed and approximate vehicle weight. Compared to existing inductive loop based traffic sensors, the new sensor is expected to provide increased reliability, easy installation and low maintenance costs. The sensor uses power only for wireless transmission and has ZERO idle power loss. Hence the sensor is expected to be extremely energy efficient. Energy to power this sensor is harvested entirely from the short duration vibrations that results when an automobile passes over the sensor.

A significant portion of the project focuses on developing low power control algorithms that can harvest energy efficiently from the short duration vibrations that result when a vehicle passes over the sensor. To this effect this report develops and compares three control algorithms “Fixed threshold switching”, “Maximum Voltage switching” and “Switched Inductor” for maximizing this harvested energy. The novel “Switched inductor” algorithm with a dual switch control configuration is shown to be the most effective at maximizing harvested energy. All three of the developed control algorithms can be implemented using simple low power analog circuit components.

The developed sensor is evaluated using a number of experimental tests. Experimental results show that the sensor is able to harvest adequate energy for its operation from the passing of every axle over the sensor. The sensor can reliably and accurately measure traffic flow rate.

17. Document Analysis/Descriptors	18. Availability Statement		
Traffic sensor, wireless traffic sensor, energy harvesting, battery-less wireless sensor, traffic flow measurement	No restrictions. Document available from: National Technical Information Services, Springfield, Virginia 22161		
19. Security Class (this report) Unclassified	20. Security Class (this page) Unclassified	21. No. of Pages 42	22. Price

Novel Battery-Less Wireless Sensors for Traffic Flow Measurement

Final Report

Prepared by

Krishna Vijayaraghavan
Rajesh Rajamani

Department of Mechanical Engineering
University of Minnesota

November 2008

Published by

Intelligent Transportation Systems Institute
Center for Transportation Studies
University of Minnesota
200 Transportation and Safety Building
511 Washington Ave SE
Minneapolis, Minnesota 55455

ACKNOWLEDGMENTS

The author(s) wish to acknowledge those who made this research possible. The study was funded by the Intelligent Transportation Systems (ITS) Institute, a program of the University of Minnesota's Center for Transportation Studies (CTS). Financial support was provided by the United States Department of Transportation Research and Innovative Technologies Administration (RITA).

TABLE OF CONTENTS

I. Review of Current Traffic Sensors 1
II. New Battery-Less Wireless Traffic Sensor 2
A. Overview 2
B. Principle 2
C. Hardware 2
D. Controller Constraint 4
E. System Model for Control 4
III. Control System Design and Analysis 7
A. Fixed Threshold Switching 8
B. Max Voltage Switching 10
C. Switched Inductor 13
D. Effect of MOSFET on "Switched Inductor" 18
E. Comparison of Control Algorithms 21
IV. Experimental Results 22
V. Traffic Sensor Networks 26
A. Introduction 26
B. Encoder Decoder 26
C. Experimental Results 27
VI. Completion of Project Tasks 31
A. Full Sensor Vs Basic Sensor 31
B. Use of SAW Device for Battery-Less Wireless Operation 32
VII. Conclusions 33
References 34

LIST OF FIGURES

Figure 1: Photograph of Sensor Based on the First Design **3**
Figure 2: Photograph of Re-Designed Sensor **3**
Figure 3: Sensor Dimensions **4**
Figure 4: Energy Harvesting Circuit **6**
Figure 5: Force Input Used for Simulation **7**
Figure 6: Mechanical Response of the System **8**
Figure 7: State Transition Diagram for "Fixed Threshold Switching" **8**
Figure 8: Voltage Output for "Fixed Threshold Switching" Algorithm **9**
Figure 9: Load Current for 1K Load with "Fixed Threshold Switching" Algorithm **9**
Figure 10: Instantaneous Power Consumed by 1K Load with "Fixed Threshold Switching Algorithm" **9**
Figure 11: State Transition Diagram for "Max Voltage Switching" **10**
Figure 12: Voltage Output for "Max Voltage Switching Algorithm" **12**
Figure 13: Load Current for 1K Load with "Max Voltage Switching Algorithm" **12**
Figure 14: Instantaneous Power Consumed by 1K Load with "Max Voltage Switching Algorithm" **13**
Figure 15: Energy Harvesting with Inductor **14**
Figure 16: State Transition Diagram for SW_L ("Switched Inductor") **14**
Figure 17: State Transition Diagram for SW_P ("Switched Inductor") **14**
Figure 18: Voltage Output for "Switched Inductor" Algorithm **17**
Figure 19: Load Current for 1K Load with "Switched Inductor" Algorithm **17**
Figure 20: Instantaneous Power Consumed by 1K Load with "Switched Inductor" **17**
Figure 21: Mosfet in Max Switch **19**
Figure 22: Simulation Results **19**
Figure 23: Results from Two Sets of Experiments **20**
Figure 24: Theoretical Voltage Obtained from Switched Inductor vs the Theoretical Voltage Obtained from Max Switching Algorithm **20**
Figure 25: "Fixed Threshold Algorithms" with a Threshold of 2.75V **22**
Figure 26: "Max Switching Algorithm" **23**
Figure 27: "Switched Inductor Algorithm" **23**
Figure 28: Max Switching **24**
Figure 29: Switched Inductor **24**
Figure 30: Capacitor Voltage Dependent on Vehicle Weight (Left: Car Driven Close to the Center @12.5 mph; Right: Motorcycle Driven Close to the Center @12.5mph) **25**
Figure 31: Circuit Schematic **27**
Figure 32: Storage Capacitor Voltage (1^{st} Configuration of Encoder) **28**
Figure 33: Decoder Output (1^{st} Configuration of Encoder) **29**
Figure 34: Storage Capacitor Voltage (2^{nd} Configuration of Encoder) **29**
Figure 35: Decoder Output (2^{nd} Configuration of Encoder) **30**

EXECUTIVE SUMMARY

This project presents a novel battery-less wireless sensor that can be embedded in the road and used to measure traffic flow rate, speed and approximate vehicle weight. Compared to existing inductive loop based traffic sensors, the new sensor is expected to provide increased reliability, easy installation and low maintenance costs. The sensor uses power only for wireless transmission and has ZERO idle power loss. Hence the sensor is expected to be extremely energy efficient. Energy to power this sensor is harvested entirely from the short duration vibrations that results when an automobile passes over the sensor.

A significant portion of the project focuses on developing low power control algorithms that can harvest energy efficiently from the short duration vibrations that result when a vehicle passes over the sensor. To this effect this paper develops and compares three control algorithms "Fixed threshold switching", "Maximum Voltage switching" and "Switched Inductor" for maximizing this harvested energy. The novel "Switched inductor" algorithm with a dual switch control configuration is shown to be the most effective at maximizing harvested energy. All three of the developed control algorithms can be implemented using simple low power analog circuit components.

The developed sensor is evaluated using a number of experimental tests. Experimental results show that the sensor is able to harvest adequate energy for its operation from the passing of every axle over the sensor. The sensor can reliably and accurately measure traffic flow rate. The width of the wireless transmission pulse from the sensor is roughly proportional to the weight of the vehicle passing over the sensor. Thus the vehicle weight can be approximately measured. Each sensor is provided with a uniquely identified encoder that enables the receiver to identify the specific sensor from which it receives wireless transmission. This will enable networking of multiple sensors (at intersections and on highways) with a single transceiver.

I. REVIEW OF CURRENT TRAFFIC SENSORS

Transportation agencies all around the country monitor traffic flow rates on most major highways using inductive loop detectors (ILDs). The Minnesota Department of Transportation (MnDOT) for example, monitors the flow rates at over 6000 points in the Minneapolis/St. Paul metro area using such ILDs. An ILD consists of a big loop of metallic coil buried in the lane. This loop is connected to a station which powers the loop and processes the information obtained from the loop to determine if a vehicle passes over the sensor. The flow rate information from such sensors is used to control ramp meters, identify congestion points, detect incidents and for a number of other applications.

Inductive loop detectors exhibit high accuracy in detecting vehicles ([27]). Thus despite various new non-intrusive technologies for detecting vehicles such as image processing based detectors ([5],[8],[13],[15]) and systems based on audio processing ([1], [2]), inductive loop detectors remain the most widely used technology.

Despite their popularity, ILDs are far from perfect and there has been considerable work to improve detection using better models, better filtering technology and by using better identification techniques such as Fuzzy Logic and Artificial Neural Networks (ANNs) ([1], [11], [25]). Despite many improvements, the installation of the ILD involves cutting a large section of the roadway in each lane and therefore causes considerable traffic disruption. Owing to its operating principle, the ILD needs to be continuously powered resulting in considerable idle power loss. For example, an ILD needs to be continuously powered during the night, even if there is very little traffic flowing on a particular highway.

Research continues to be done on development of other new traffic sensors. The Hi-Star portable traffic sensor from Quixote Transportation Technologies is a portable traffic analyzer that can be placed on the road surface in the traffic lane and connected to a computer for data retrieval. It is useful for applications where a temporary traffic sensor is required, for example for conducting traffic and turn analysis at an intersection or for surveying traffic on a bridge or parking garage.

The traffic sensor developed in this project is unique and different from all the sensor technologies described above. Its uniqueness comes from the fact that it is the first ever sensor that is battery-less, wireless and is powered entirely by harvesting energy from vibrations for its operation.

II. NEW BATTERY-LESS WIRELESS TRAFFIC SENSOR

A. Overview

This project has developed a novel battery-less wireless traffic sensor, which is extremely energy efficient. The sensor is completely autonomous and can be embedded in the lane without the need for control/data cables. In the absence of any automobile, the sensor is completely turned off, consuming no power. Thus, the sensor has ZERO idle power loss. When an automobile passes over the sensor, the sensor is turned on and a RF pulse is transmitted wirelessly to the station. The sensor requires no external power source as it is powered by harvesting all its energy from vibrations that result when a vehicle passes over it. Further this sensor has smaller dimensions and can be installed with much lower traffic disruptions. This is especially true because the sensor does not need a power source and power lines do not need to be run to the sensor. This new sensor, like the ILD, does not use complex image processing or audio processing techniques and would hence provide the same level of high reliability. Owing to the battery-less and wireless nature of the sensor low maintenance can also be expected. Further the sensor can measure the number of axles and the approximate weight of the passing vehicle in addition to the traffic flow rate. It is also possible to configure several sensors to transmit to a single station by transmitting a unique code using a programmed encoder.

B. Principle

The proposed sensor is based on the principle of vibration harvesting energy (VHE) to enable wireless transmission of signals. Sodana et. al (2004) ([24]) provides a good review of many of these VHE techniques. Some of the earlier work has also focused on developing control algorithms to optimize the amount of energy harvested ([14], [20]). However, the VHE techniques in literature focus predominantly on harvesting energy from a continuous source of vibration. When a vehicle passes over the sensor, the resulting vibrations mechanical are of short duration. Hence, although the concept of VHE is not new, it has never before been used to power a traffic sensor. Further the optimal algorithms that have been proposed earlier cannot be implemented in a stand-alone sensor as they require an external control input (and possibly an external power source). Hence new algorithms have been developed and implemented in this project.

C. Hardware

The proposed sensor consists of a double beam structure with a main beam and two additional support beams. The first sensor designed by the team was essentially a two-dimensional structure with the two lower support beams being perpendicular to the main beam. A photograph of this sensor is shown in figure 1.

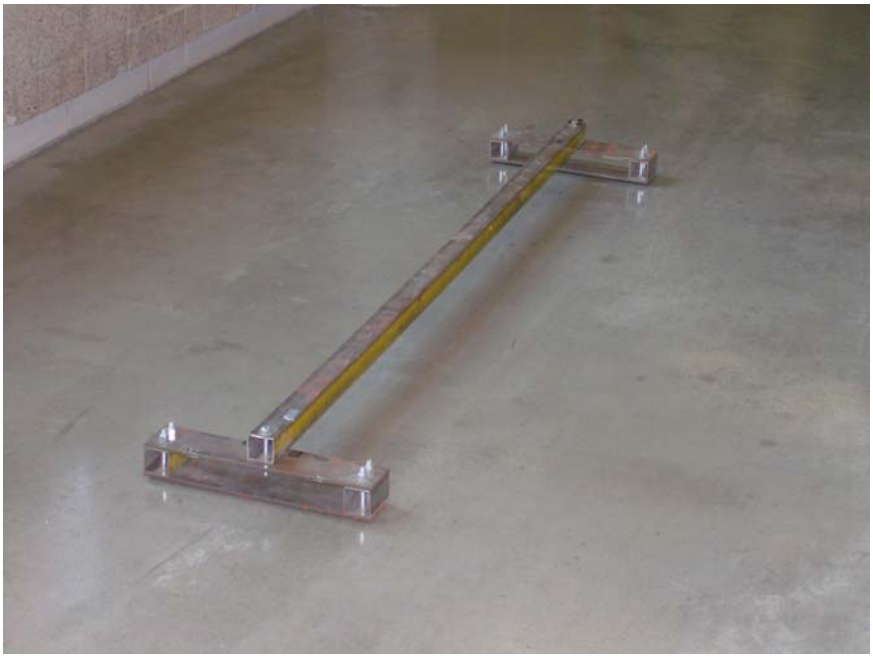

Figure 1: Photograph of Sensor Based on the First Design

This sensor was later replaced by a much more compact design in which the two lower beams are along the same axis as the upper main beam. This leads to an essentially one-dimensional structure. A photograph of the re-designed one-dimensional sensor is shown in figure 2.

Figure 2: Photograph of Re-Designed Sensor

The main beam of the sensor is 6’ (or 1.8 meters) long and the two support beams are 10” long (or 250 mm) at the ends. A schematic of the sensor with dimensions is shown in figure 3. A total of eight Piezo elements (four piezos for each of the support beams) are bonded at the locations shown in figure 3 and connected electrically in parallel. Finite element simulations using ANSYS revealed that the average of the strain over the area of all the piezos depended only on the total load acting on the main beam. The double layer beam configuration was chosen since the average voltage developed by the piezo would be independent of the lateral location of the load and the sensor can thus determine the weight of the passing vehicle. It should be noted further that the speed of the passing vehicle can be measured by measuring the time difference in the loading between two consecutive sensors placed a short longitudinal distance apart. Since each axle applies a distinct load on the sensor, the number of axles on the vehicle can be counted.

D. Controller Constraint

In this paper, we develop a controller to optimize energy harvested from short duration inputs from near impact loading. This technique could be extended to harvest energy from other sources such as shock absorbers and landing gear in airplanes during touch down. The emphasis on this paper has been on developing control strategies for the Energy Harvesting Systems (EHS) that are completely powered from the energy that is harvested. The design has been restricted to a controller that can be implemented using simple onboard analog electronics. The efficacy of these control strategies have been verified using simulations and experiments.

E. System Model for Control

The EHS consists of piezo electric substrate bonded to a beam structure as shown in figure 3. When a vehicle passes over the sensor, the piezo experiences a strain from the loading. The strain on the piezo results in a voltage being developed in the piezo. This piezo voltage causes a reaction force on the beam structure. This force would couple the mechanical dynamics of the beam structure with the electrical dynamics. However the Piezo element has a cross-section of 25mm×0.191mm which is much smaller cross section of the parent material. Hence the force generated by the piezo can be neglected in calculating the overall strain, effectively decoupling the mechanical dynamics from the electrical dynamics. The overall dynamics of the system can be modeled as a cascaded dynamics system.

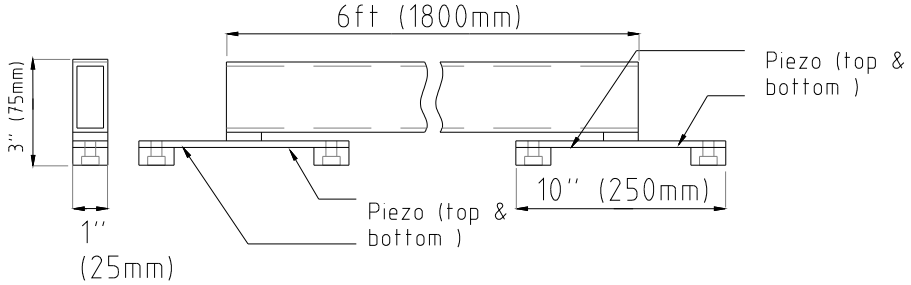

Figure 3: Sensor Dimensions

The mechanical system that drives the electrical system consists of the vibrating beam structure. For a simple beam structure in vibration, the various modes of vibration can be calculated using equation (1). More complicated structures require a FEM model solution.

$$\rho A \frac{\partial^2 v(x,t)}{\partial t^2} + b \frac{\partial v(x,t)}{\partial t} + EI \frac{\partial^4 v(x,t)}{\partial x^4} = 0 \qquad (1)$$

The dominant frequencies thus obtained can be used to construct a low order system model. Thus for the purposes developing the control system, the mechanical system can be considered to be a spring mass damper system with the equation (2) and the strain is calculated from equation (3)

$$\ddot{u} + 2\zeta\omega_n \dot{u} + \omega_n{}^2 u = \frac{F}{m} \qquad (2)$$

$$\varepsilon = \frac{u}{l} \qquad (3)$$

where

u is the displacement of the mechanical system

l is the length scale associated with the mechanical system.

At low frequencies, the Piezo electric material which is the critical part of the EHS, is modeled as a voltage source in series with a capacitance using equation (4) & (5) ([4], [18]). A more sophisticated model can be found in Weinbert et. al.([29]).

$$V_{piezo} = V_{strain} - \frac{1}{C_{piezo}} \int i_p dt \qquad (4)$$

$$V_{strain} = \delta \varepsilon / d \qquad (5)$$

where

V_{piezo} is the voltage measured across the Piezo,

V_{strain} is the voltage open circuit voltage generated due to the strain

C_{piezo} is the capacitance of the Piezo

i_p is the current through the Piezo

d is the Piezo constant defined as the strain developed per unit applied electrical field

δ is the thickness of Piezo

ε is the strain in the Piezo, from eq. (3)

The electrical system shown in figure 4 also consists of a bridge rectifier (denoted by "Diode Bridge") connected to the Piezo element. The diode bridge is connected to a storage capacitor C_s, which in turn is connected to transmitter via a load switch (SW_L). The transmitter is modeled as a load resistor R_L in the circuit. The control circuit is not included in the dynamics owing to its extremely small current consumption.

In order to calculate the overall electrical dynamics, each diode making up the bridge is modeled by a piecewise linear model ([22]). The piezo current i_p can then be written as equation (6) and the dynamics of the capacitor voltage can be given by equation (7).

$$i_p = \begin{cases} \dfrac{|V_{piezo}| - V_{Cs} - 2V_d}{R_d} \times sign(V_{piezo}) & \\ \qquad\qquad if \quad |V_{piezo}| > |V_{Cs} + 2V_d| & \\ 0 \qquad\qquad otherwise & \end{cases} \quad (6)$$

$$\begin{aligned} C_s \dot{V}_{Cs} + 1/R_L V_{Cs} &= |i_p| \qquad if \ SW_L \ is \ closed \\ C_s \dot{V}_{Cs} &= |i_p| \qquad if \ SW_L \ is \ open \end{aligned} \quad (7)$$

where

V_d is the forward voltage drop across each diode
(about 0.7 V to 1.1 V based on the type of diode used)

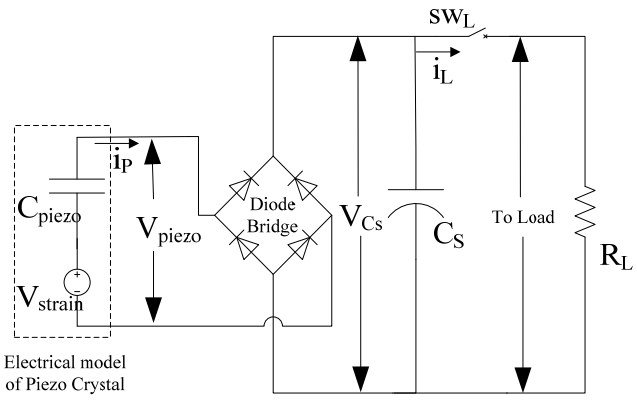

Figure 4: Energy Harvesting Circuit

III. CONTROL SYSTEM DESIGN AND ANALYSIS

Of the total energy generated in the Piezo, only the fraction transferred to the storage capacitor C_s is available to drive the load. This energy can be calculated in terms of the maximum voltage across the storage capacitor C_s as $V_{Cs}^{\max}$. In the following section, the available voltage is determined for each of three different control algorithms. For the purpose of simulation, we consider the mechanical system with a mass of 100Kgs, a damping ratio of 0.7 and a spring constant of 10^6 N/m. These parameters were chosen so as to provide a natural frequency of 100 Hz in the simplified mechanical model. The load is shown in figure 5, and the response of the mechanical system is seen in figure 6. The system was designed so that the Piezo would produce $V_{strain} = 60V$ for the static weight of the automobile. The load switch, SW_L, shown in figure 4 is implemented using a MOSFET transistor.

The load resistor is of the order of $1K\Omega$. If SW_L is always closed, this load resistor is always connected to the Piezo. In fact by using equations (4-7) in a Simulink model, it can be shown that the peak magnitude of V_{Cs} would be $1.7V$. This voltage cannot drive the transmitter, which requires a supply of $2.5V$ at the very least.

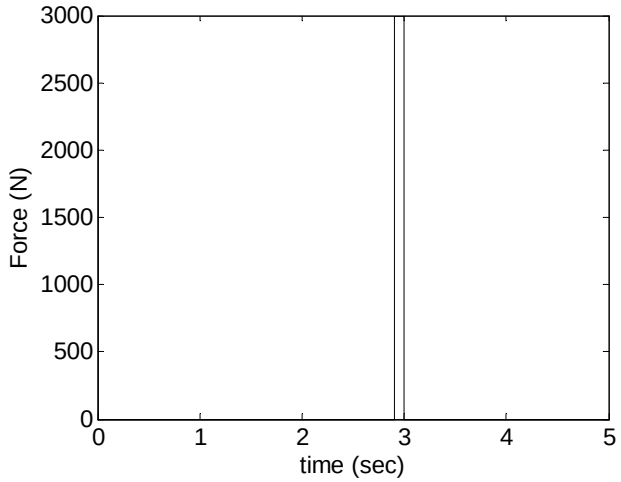

Figure 5: Force Input Used for Simulation

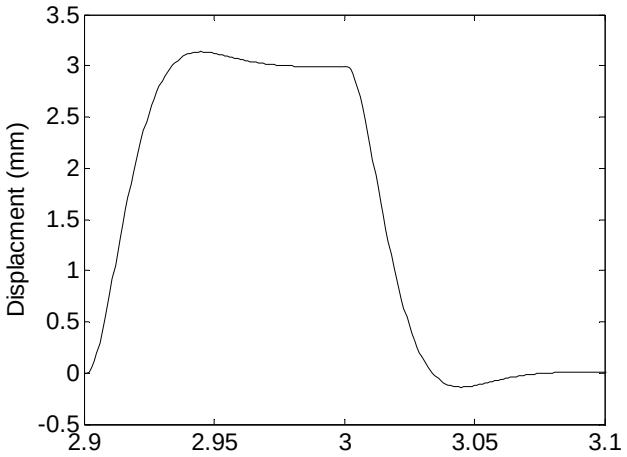

Figure 6: Mechanical Response of the System

A. Fixed Threshold Switching

This is an existing algorithm for energy harvesting and the simplest [21]. In this algorithm, the load is connected to the storage capacitor (C_s), by setting the control input to logic high (1) when the voltage across this capacitor (V_{Cs}) crosses a predetermined on-threshold V_{high}. The control is turned off (0), if V_{Cs} falls below an off-threshold V_{low}. The control signal to SW_L, can be given by the control law state transition diagram shown in figure 7.

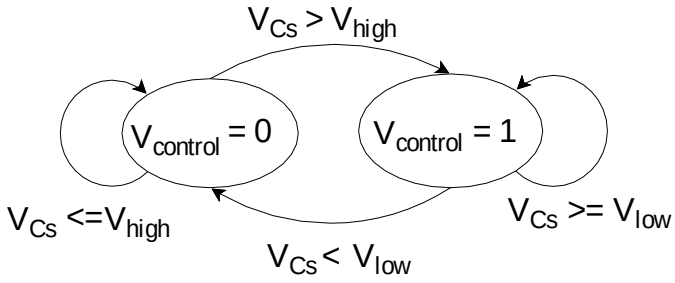

Figure 7: State Transition Diagram for "Fixed Threshold Switching"

Once the load switch SW_L is closed, the voltage across the storage capacitor V_{Cs} does not build any further. The maximum of value $V_{Cs}^{\max}$ is equal to the on-threshold V_{high}. The fixed threshold switching is the simplest algorithm, and would serve as a baseline for evaluating the performance of the other control algorithms. Simulation results obtained using this baseline control law is shown below. The voltage in the storage capacitor is seen in figure 8, while figure 9 and figure 10, respectively, show the instantaneous load current and power at the load.

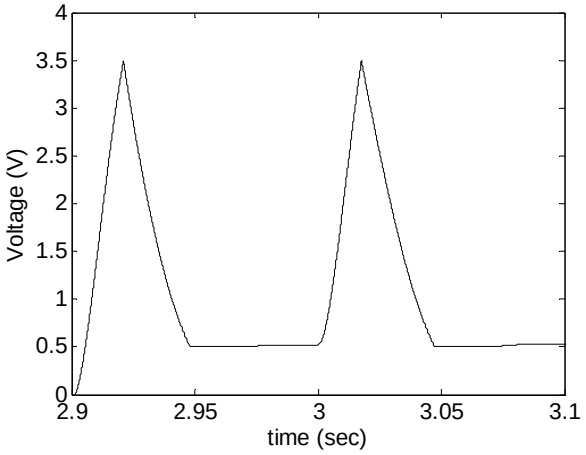

Figure 8: Voltage Output for "Fixed Threshold Switching" Algorithm

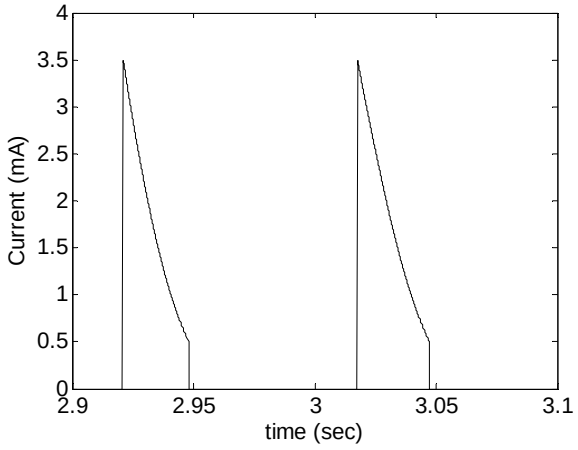

Figure 9: Load Current for 1K Load with "Fixed Threshold Switching" Algorithm

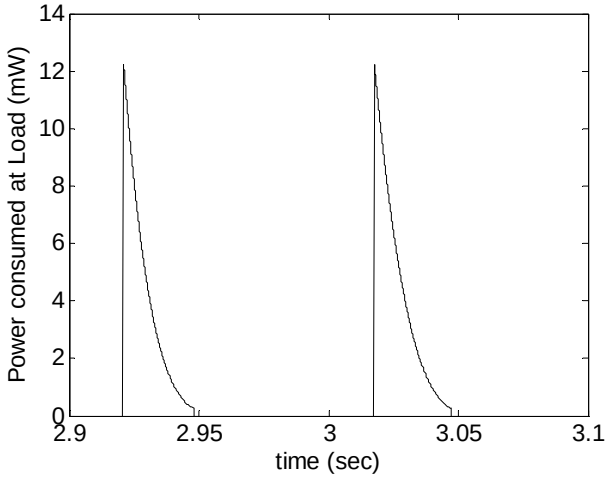

Figure 10: Instantaneous Power Consumed by 1K Load with "Fixed Threshold Switching Algorithm"

B. Max Voltage Switching

In this new algorithm, the load is connected to the storage capacitor (C_s), when the voltage across this capacitor (V_{Cs}) reaches a maximum value. The control SW_L is turned off, if V_{Cs} falls below the off-threshold V_{low}. The control law can be given by the state transition diagram shown in figure 11. The occurrence of maximum can be determined using analog electronics. For instance, the max-detector can be realized using a high pass RC filter given by equations (8) . A maximum is declared when the output of this filter falls below a threshold. The value of this threshold is small and determines how close to zero the derivative must become for the voltage to be recognized as maximum.

$$V_{filter} = \frac{RCs}{RCs+1} V_{Cs} \qquad (8)$$

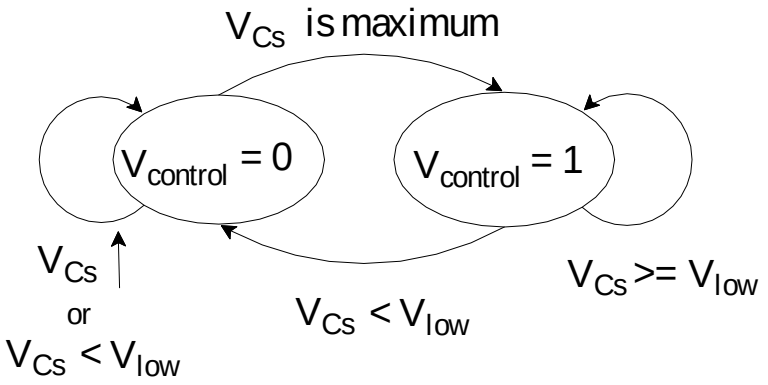

Figure 11: State Transition Diagram for "Max Voltage Switching"

If the displacement of the beam has only one extremum value $u_{\max}$ (with a corresponding $V_{strain} = V_{strain}^{\max}$), then $V_{Cs}^{\max}$ can be calculated using

$$V_{Cs}^{\max} = \begin{cases} \left(\frac{C_{piezo}}{C_s + C_{piezo}} \right) \times \left(\left| V_{strain}^{\max} \right| - 2V_d \right) & if \quad \left| V_{strain}^{\max} \right| > 2V_d \\ 0 & otherwise \end{cases} \qquad (9a)$$

$$\left| V_{Cpiezo}^{\max} \right| = \begin{cases} \left(\frac{C_s}{C_s + C_{piezo}} \right) \times \left(\left| V_{strain}^{\max} \right| - 2V_d \right) & if \quad \left| V_{strain}^{\max} \right| > 2V_d \\ 0 & otherwise \end{cases} \qquad (9b)$$

Thus for a sufficiently large strain voltage, the difference between $V_{strain}^{\max}$ and $2 \times V_d$ is distributed between C_s and C_{piezo} in the inverse ratio of their capacitance.

It must be noted that for the "Fixed Threshold Switching" algorithm to work reliably, V_{high} needs to be chosen to detect every single vehicle. Hence V_{high} must be chosen a volt or two lower than the lowest $V_{Cs}^{\max}$ obtained from (9) corresponding to the smallest $V_{strain}^{\max}$. Thus, although it is not directly evident, $V_{Cs}^{\max}$ obtained from "Max Voltage Switching" algorithm is necessarily larger than that obtained from "Fixed Threshold Switching" algorithm.

Equation (9) can be derived as follows. It is clear that $V_{strain} = V_{piezo} + V_{Cpiezo}$ (refer figure 4). Thus if $\left|V_{strain} - V_{Cpiezo}\right| - V_{Cs} > 2V_d$, the bridge circuit rectifies the piezo current and charges the storage capacitor. When $\left|V_{strain} - V_{Cpiezo}\right| - V_{Cs} \le 2V_d$, the diodes block the flow of current thus preventing storage capacitor from discharging. If i_p does not change signs and $\left|V_{strain} - V_{Cpiezo}\right| - V_{Cs} > 2V_d$, the effective voltage driving the current thought the resistive element in the circuit is given by

$$V_{effective}(t) = sign\left(V_{strain}(t) - V_{Cpiezo}(t)\right) \times \max\left(\left|V_{strain}(t) - V_{Cpiezo}(t)\right| - V_{Cs}(t) - 2V_d, 0\right) \quad (10)$$

In modeling overall dynamics, the first order nonlinear electrical dynamic equations (4-7) are dominated by the much slower dynamics of the mechanical system. The system exhibits a two time scale property and the faster electrical dynamics needs to be modeled by its quasi-steady state value ([9], [12]) which corresponds to $V_{effective}(t) = 0$. Equivalently

$$\left|V_{strain}(t) - V_{Cpiezo}(t)\right| = V_{Cs}(t) - 2V_d \quad (11)$$

Since C_s and C_{piezo} are two capacitor connected in series, as long as $\dot{V}_{strain}(t)$ does not change signs

$$\frac{\left|V_{Cpiezo}(t)\right|}{V_{Cs}(t)} = \frac{C_s}{C_{piezo}} \quad (12)$$

Thus

$$V_{Cs} = \begin{cases} \left(\frac{C_{piezo}}{C_s + C_{piezo}}\right) \times \left(\left|V_{strain}\right| - 2V_d\right) & if \quad \left|V_{strain}\right| > 2V_d \\ 0 & otherwise \end{cases}$$

$$\left|V_{Cpiezo}\right| = \begin{cases} \left(\frac{C_s}{C_s + C_{piezo}}\right) \times \left(\left|V_{strain}\right| - 2V_d\right) & if \quad \left|V_{strain}\right| > 2V_d \\ 0 & otherwise \end{cases} \quad (13)$$

The above equation directly yields equation (9).

For the current setup, with $V_{strain}^{\max} = 62$, $C_{piezo} = 850nF$, $C_s = 10\mu F$, $V_{strain}^{\max}$ is calculated to be $4.82V$.

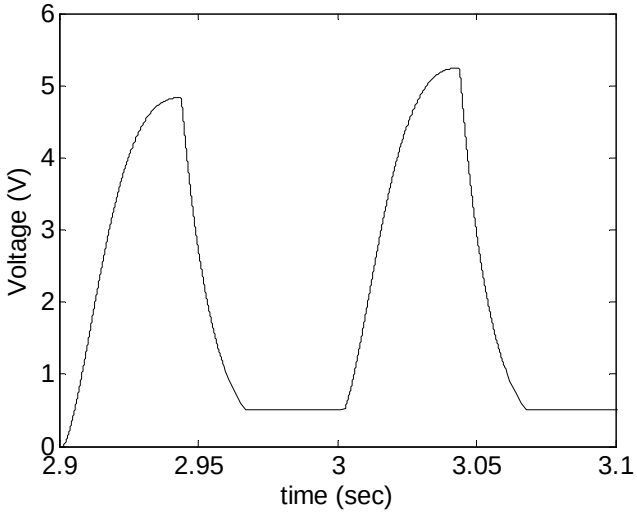

Figure 12: Voltage Output for "Max Voltage Switching Algorithm"

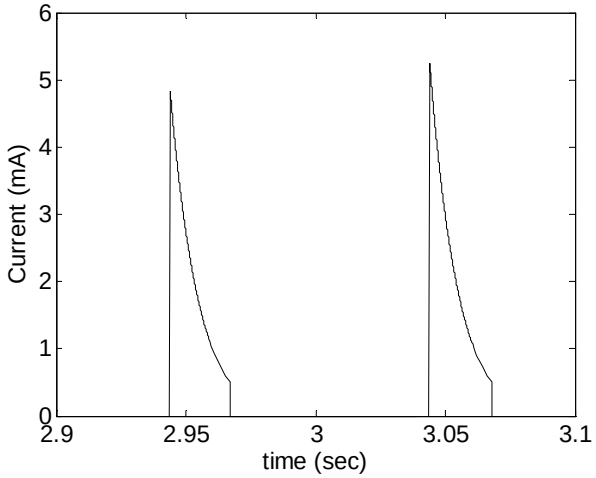

Figure 13: Load Current for 1K Load with "Max Voltage Switching Algorithm"

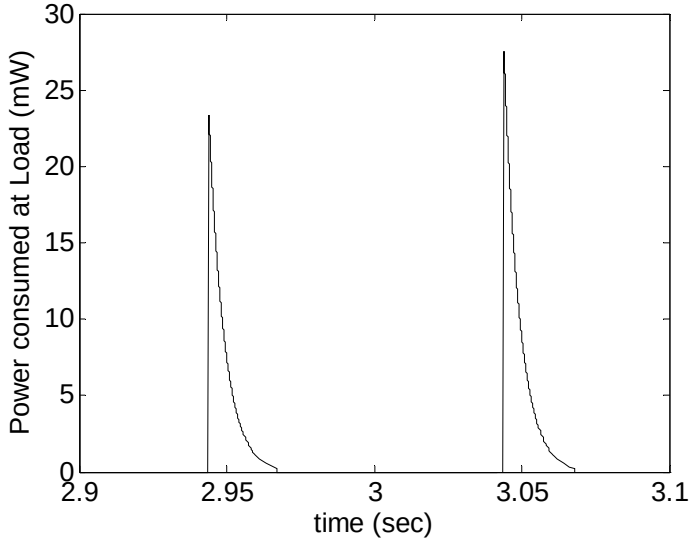

Figure 14: Instantaneous Power Consumed by 1K Load with "Max Voltage Switching Algorithm"

Since the storage capacitor is allowed to charge to a higher voltage, this algorithm delivers a larger peak power in comparison to the "Fixed Threshold switching". It is seen that the maximum power of the "Max Voltage Switching" (figure 14) is nearly twice the maximum power of the "Fixed Threshold switching" (figure 10). By virtue of its design, V_{high} for fixed threshold algorithm, need to be necessarily chosen to be less than the value of V_{Cs} obtained from equation (9) for the lightest vehicle. Hence this algorithm is always more efficient at harvesting vibration energy than the simple fixed threshold algorithm described in the previous section.

C. Switched Inductor

This section proposes a third algorithm that would further enhance $V_{Cs}^{\max}$. This algorithm uses a circuit shown in figure 15. The new circuits uses an inductor (L) and piezo switch SW_P in addition to the components shown in figure 4. The voltage drop across L is given by V_L. SW_P is turned on when $|V_{piezo}|$ reaches a maximum and SW_L is turned on when V_{Cs} reaches a maximum. The switches SW_P and SW_L are turned off when the respective voltages $|V_{piezo} + V_L|$ and V_{Cs} drops below an off-threshold V_{low} As discussed in the previous section, the occurrence of maximum can be determined using analog electronics. The control law for SW_P is given by state transition diagram shown in figure 16 and the control law for SW_L is given by state transition diagram state transition diagram shown in figure 17.

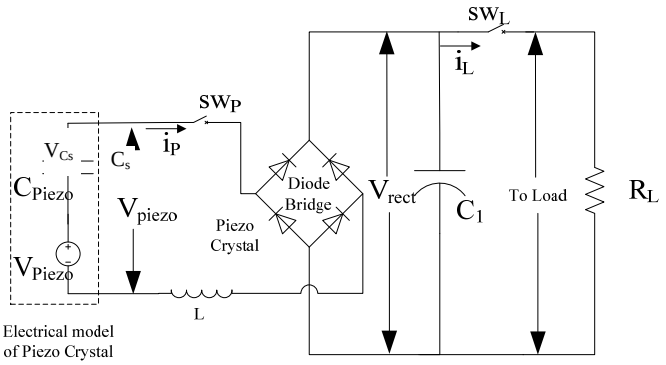

Figure 15: Energy Harvesting with Inductor

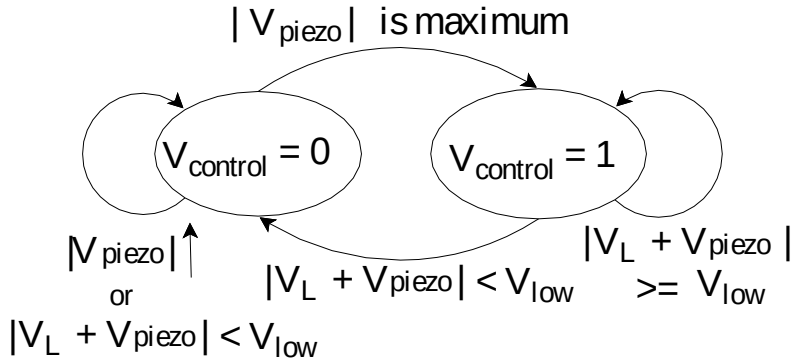

Figure 16: State Transition Diagram for SW_L ("Switched Inductor")

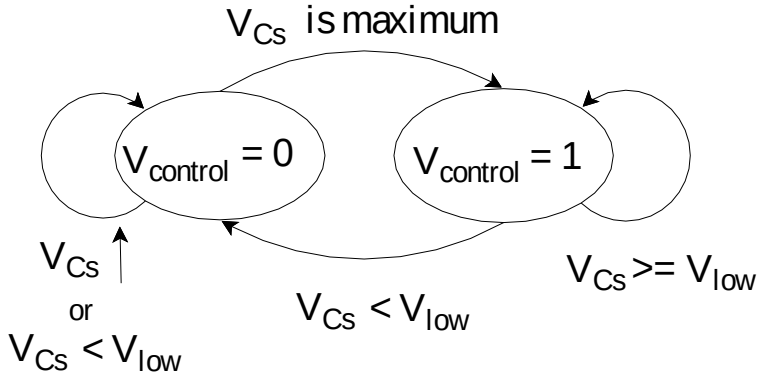

Figure 17: State Transition Diagram for SW_P ("Switched Inductor")

If the displacement of the beam has only one extremum value, then $V_{Cs}^{\max}$ can be given by

$$V_{Cs}^{\max} = \begin{cases} \left(\frac{mC_{piezo}}{C_s + C_{piezo}} \right) \times \left(\left| V_{strain}^{\max} \right| - 2V_d \right) & if \quad \left| V_{strain}^{\max} \right| > 2V_d \\ 0 & otherwise \end{cases} \tag{14}$$

where

$$m = 1 + \exp\left(-\pi \left(\zeta / \sqrt{1-\zeta^2} \right) \right), \; 1 \le m \le 2$$

$$\zeta = R_d \sqrt{\frac{C}{L}}$$

$$C = \frac{C_p C_s}{C_p + C_s}$$

By comparing equations (14) with (9), we notice that $V_{Cs}^{\max}$ has increased by a factor $(m-1)$, which equals the peak overshoot of the LCR circuit. The "Switched Inductor" algorithm yields a higher $V_{Cs}^{\max}$ due to the presence of the inductor. In the absence of the diode bridge rectifier, the second dynamics of the LCR circuit will exhibit an oscillatory behavior for an extremely small time period dt and the dynamics would eventually converge to its steady state value. The bridge rectifier in the circuit would however clamp V_{Cs} to the overshoot voltage, resulting in higher available voltage.

Equation (14) can be derived as follows. When SW_P is closed, the circuit is similar to the circuit in section III B, and the effective voltage driving the resistive and inductive components of the circuit is given by

$$\begin{aligned} V_{effective}(t) = sign\left(V_{strain}(t) - V_{Cpiezo}(t) \right) \times \\ \max\left(\left| V_{strain}(t) - V_{Cpiezo}(t) \right| - V_{Cs}(t) - 2V_d, 0 \right) \end{aligned} \tag{15}$$

In the absence of SW_P, the overall dynamics is dominated by the mechanical system and $V_{Cs}^{\max}$ would be given by equation (9). There would be no gain in V_{Cs}. If SW_P is closed at some $t = t_0$ when $V_{strain} = V_{strain}^0$, it would be result in a step input to the electrical circuit. If $|V_{strain}(t_0)| > 2V_d$, the diode bridge will begin to conduct when SW_P is closed.

$$L\frac{di_p}{dt} + 2R_d i_p = V_{effective}(t_0) \tag{16}$$

When i_p is unidirectional, the electrical dynamics can be written in terms of $Q = \int i_p dt$ and $|Q| = \int |i_p| dt$. Substituting

$$V_{Cpiezo} = \frac{1}{C_{piezo}} \int i_p dt = \frac{Q}{C_{piezo}} \tag{17}$$

$$V_{Cs} == \frac{1}{C_{piezo}} \int |i_p| dt = \frac{|Q|}{Cs} \tag{18}$$

and noting that $sign\left(V_{strain}^{0}\right) = sign(Q)$, the piece-wise linear dynamics of the LCR system can be written as

$$\begin{aligned} &L\ddot{Q} + 2R_d \dot{Q} + \left(1/C_{piezo} + 1/C_s\right)Q \\ &= V_{strain}^{0} - 2V_d \times sign\left(V_{strain}^{0}\right) \end{aligned} \tag{19}$$

Now $i_p = \dot{Q}$ and i_p is unidirectional up to the first maximum of Q. Since equation (19) is valid when i_p is unidirectional, it can be used to determine this first maximum $Q_{\max}$. For this second order system,

$$Q_{\max} = C \times m \times V_{strain}^{0} \tag{20}$$

Closing SW_P when V_{piezo} is maximum, would result in step voltage input the electrical LCR circuit (equal to $V_{strain}^{\max}$). Thus

$$V_{Cs}^{\max} = \begin{cases} \left(\dfrac{mC_{piezo}}{C_s + C_{piezo}}\right) \times \left(\left|V_{strain}^{\max}\right| - 2V_d\right) & if \quad \left|V_{strain}^{\max}\right| > 2V_d \\ 0 & otherwise \end{cases} \tag{21}$$

Simulation results using the switched inductor controller are shown in the following figures. When compared to the "Max voltage switch" controller, it is seen from figure 12 and figure 18 that the available voltage has increased by a factor of over 2.5, and from figure 14 and figure 20, it is seen that peak power is increased by a factor of 6. Using equation (31) to (34), a value of $V_{Cs} = 9.45V$ is obtained for the first pulse. The estimated value for V_{Cs} is seen to be in close agreement with the simulation result from figure 18.

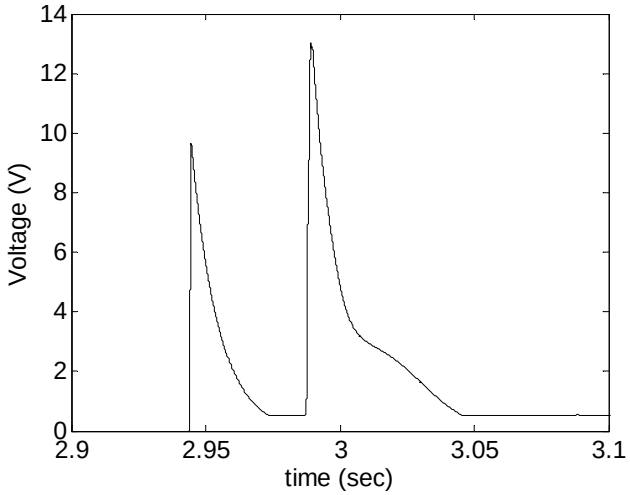

Figure 18: Voltage Output for "Switched Inductor" Algorithm

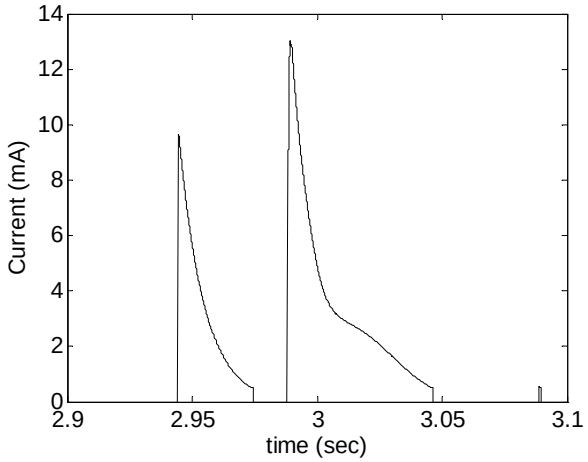

Figure 19: Load Current for 1K Load with "Switched Inductor" Algorithm

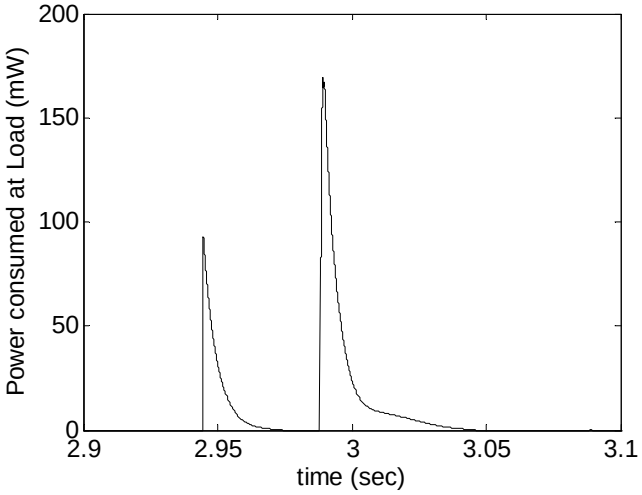

Figure 20: Instantaneous Power Consumed by 1K Load with "Switched Inductor"

D. Effect of MOSFET on "Switched Inductor"

In estimating the value of V_{Cs}, section III.C assumes ideal switches and neglects the voltage drop across SW_P. The practical realization of the max switch involves an analog electronics circuit with a mosfet. This circuit would uses the voltage V_{Cs} stored in the storage capacitor to controls a mosfet as shown in figure 21. In the "off" state, the mosfet offers nearly infinite resistance and accurately models an ideal open switch. When the mosfet is turned "on" using a control signal, it offers a finite voltage drop V_{DS} which is a function of V_{Cs}. The voltage drop V_{DS} in turn affect the electrical dynamics and the over all electrical dynamics is no longer linear. Since there are no standard solutions for this nonlinear problem, a numerical solution framework has been presented in this sub-section. This solution can be used in conjunction with section III.C to estimate the performance of the "Switched Inductor Algorithm" with greater accuracy.

For this numerical model, the individual diodes in the bridge rectifier as well as the mosfet are modeled using the standard nonlinear equation ([7]).

$$V_{diode} = V_0 \ln\left(\frac{I_{diode}}{I_S} + 1\right) + I_{diode} R_{diode} \tag{22}$$

$$I_D = \begin{cases} 0 \\ \qquad if\ V_{GS} < V_T \\ 2k\left[(V_{GS} - V_T)V_{DS} - {V_{DS}}^2/2\right] \\ \qquad if\ V_{GS} > V_T\ and\ V_{DS} < (V_{GS} - V_T) \\ k(V_{GS} - V_T)^2 \\ \qquad if\ V_{GS} > V_T\ and\ V_{DS} > (V_{GS} - V_T) \end{cases} \tag{23}$$

where the subscripts

V_{GS} refers to the source-gate voltage

V_{DS} refers to the source-drain voltage

V_T is the mosfet threshold voltage

k is a mosfet constant

Clearly

$$V_{GS} = V_{DS} + V_{Cs} \tag{24}$$

Hence

$$V_{DS} = \begin{cases} -(V_{Cs} - V_T) + \left[(V_{Cs} - V_T)^2 + I_D/K\right]^{1/2} \\ \qquad if\ V_{Cs} > V_T \\ (I_D/K)^{1/2} - (V_{Cs} - V_T) \\ \qquad otherwise \end{cases} \tag{25}$$

The parameters for the model that were obtained from the data sheets of the electronic components are given below.

$I_S = 2.7529 \times 10^{-15} A$

$V_0 = 0.0342 V$

$R_D = 1.1244\ \Omega$

$V_T = 1.2\ V$

$K = 9.685 \times 10^{-3}$

$L = 10\ mH$

$R = 11.8\ \Omega$

R is the resistance of the inductor which is added in series. figure 22 and figure 23 compare the experimental response of the system to the theoretical of the model of the system for equivalent piezo parameters of $C_p = 1\mu F$ and $V_{strain} = 50V$

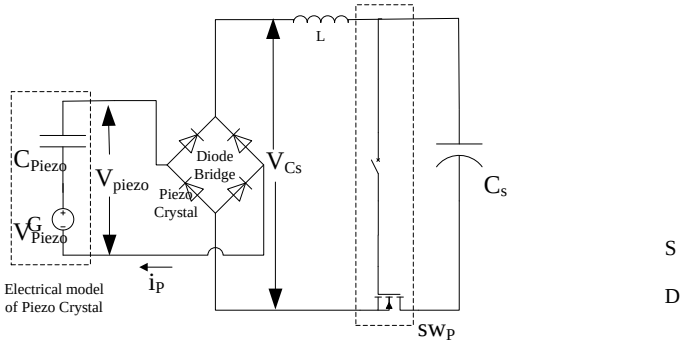

G, S and D respectively denote the gate source and drain of the mosfet

Figure 21: Mosfet in Max Switch

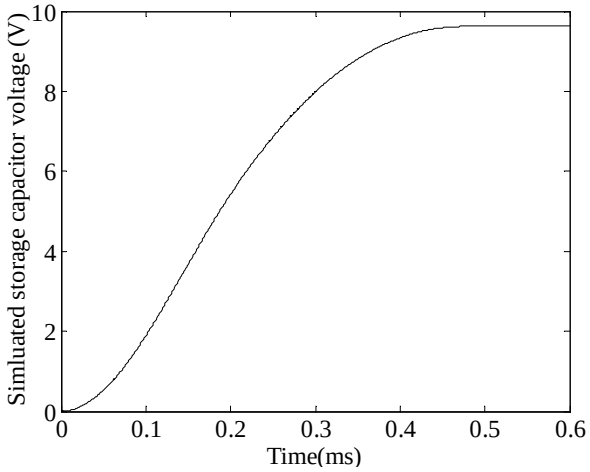

Figure 22: Simulation Results

Using this model, the theoretical voltage for the switched inductor is plotted versus the theoretical response of the max switch for the sensor in figure 24 for an initial storage capacitor voltage of 2.5V.

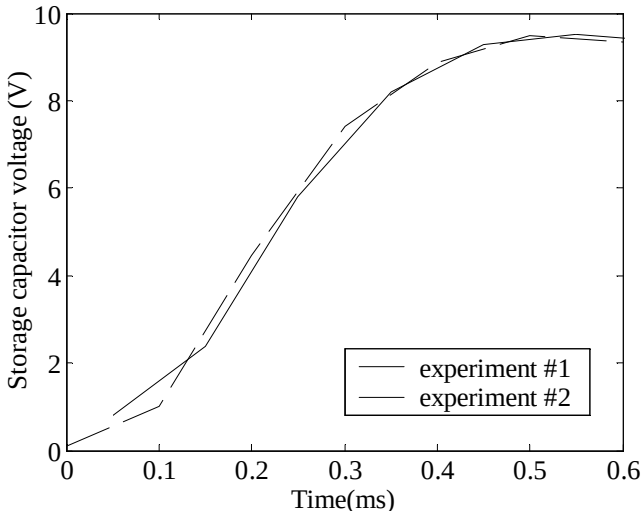

Figure 23: Results from Two Sets of Experiments

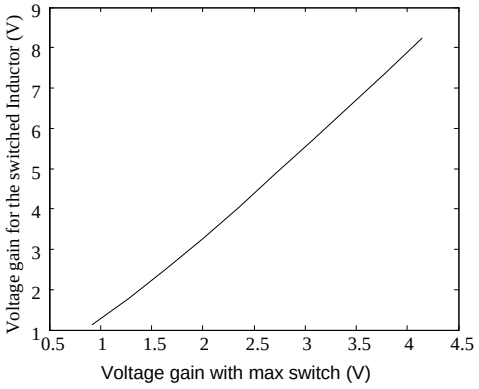

Figure 24: Theoretical Voltage Obtained from Switched Inductor vs. the Theoretical Voltage Obtained from Max Switching Algorithm

The theoretical model does not consider the equivalent series resistance of the electrolytic storage capacitor. Hence the theoretical prediction shown in figure 24 would give an upper bound for the voltage from the switched inductor algorithm.

E. Comparison of Control Algorithms

The table below shows a comparison on the maximum voltage across the storage capacitor for the three algorithms.

Algorithm	$V_{Cs}^{\max}$
Fixed Threshold Switching	V_{high}
Max Voltage Switching	$\left(\frac{C_{piezo}}{C_s + C_{piezo}}\right) \times \left(\left\|V_{strain}^{\max}\right\| - 2V_d\right)$
Switched Inductor	$\left(\frac{mC_{piezo}}{C_s + C_{piezo}}\right) \times \left(\left\|V_{strain}^{\max}\right\| - 2V_d\right)$

As noted earlier, for the "Fixed Threshold Switching" algorithm to work reliably, V_{high} must necessarily be chosen a volt or two lower than the lowest $V_{Cs}^{\max}$ obtained from equation (9) corresponding to the smallest $V_{strain}^{\max}$ that can be expected. Also, from equation 21, it is clear that $m > 1$. Thus, $V_{Cs}^{\max}$ for "Fixed Threshold" is smaller than $V_{Cs}^{\max}$ for "Max Voltage Switching" which in turn is smaller than $V_{Cs}^{\max}$ for the "Switched Inductor" algorithm.

IV. EXPERIMENTAL RESULTS

A passenger sedan car was driven over the sensor at 20 Kmph. This resulted in separate loading from the two axle, first by the front tire and then by the rear tire. For the purpose of experiments, ramps were constructed to enable the test vehicles to be driven smoothly over the sensor. Since the maximum range of our data-acquisition system was limited to $\pm 10V$, the sensor configuration was altered to limit the maximum voltage. All the experiments were performed using the same setup with only the electronic circuit being modified to realize the three control algorithms.

Figure 25 show the results from the testing of the "Fixed threshold algorithm". The on-threshold for the algorithm was chosen at 2.75 V so that the sensor would detect light vehicle such as motorcycles. The mosfet used in the switching circuit, constrain the off-threshold to 1.75V. As a result, SW_L turns on when the capacitor voltage V_{Cs} reaches 2.75V and turns off when V_{Cs} falls below 1.75V.

The electronic circuits were modified so that SW_L turns on when V_{Cs} reaches a maximum. In order to detect a global maximum, and to collect energy from both axles, SW_L was modified to turn on when V_{Cs} does not increase for a period of 100ms. The off-threshold was once again chosen to be 1.75V. Figure 26 show the results from "Max Switching algorithm".

It is seen from figure 26, that the first axle produces 1.5V and the second axle results in an additional 2.5V. The theoretical model developed in section III.D, estimates V_{Cs} when the "Switched Inductor Algorithm" is used in the place of the "Max Switching algorithm". The theoretical estimates that the first axle would produce a voltage of 2.25V and the second axle would produce 4V. It predicts an upper bound of 6.25V with the "Switched Inductor Algorithm". Figure 27 show the results from the "Switched Inductor Algorithm" experiments and the capacitor voltage is found to be 5.75V.

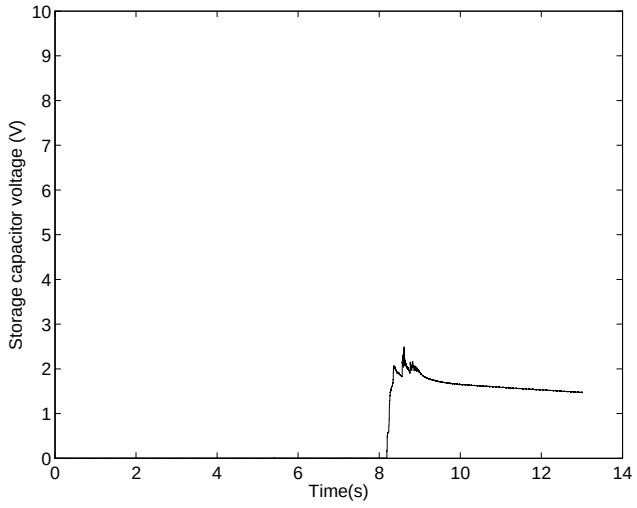

Figure 25: "Fixed Threshold Algorithms" with a Threshold of 2.75V

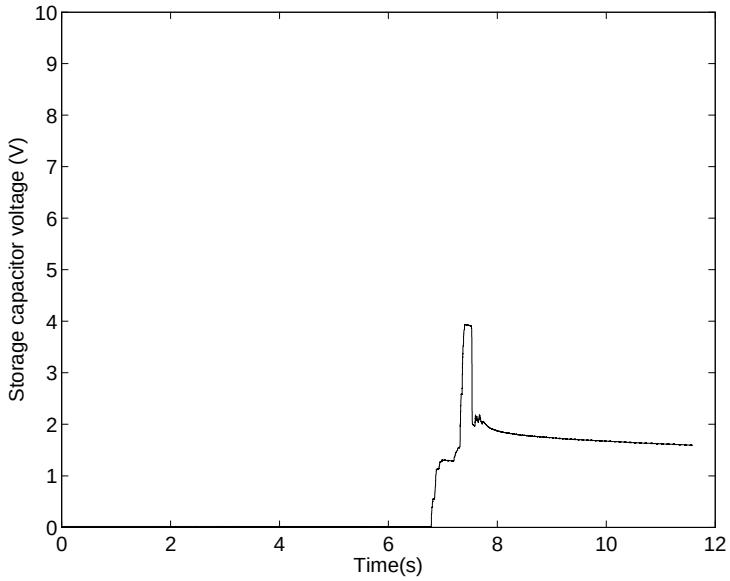

Figure 26: "Max Switching Algorithm"

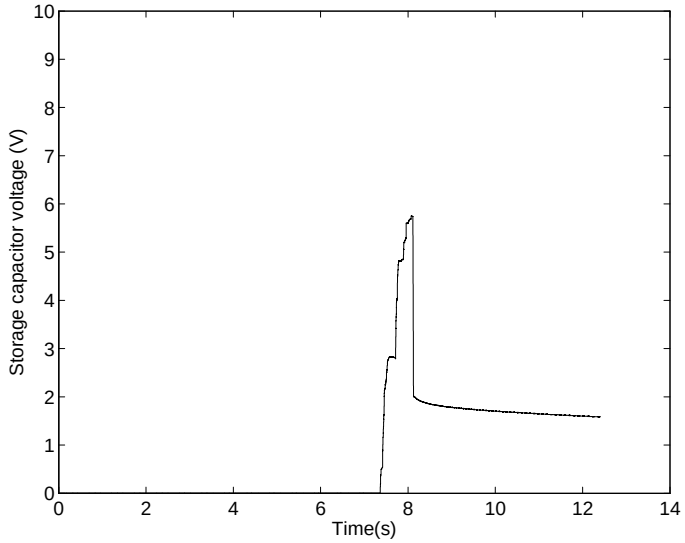

Figure 27: "Switched Inductor Algorithm"

In order to compare the energy amount of energy harvested, the load switch was disabled and the open circuit voltages generated at the storage capacitor were recorded. Figure 28 and figure 29 respectively show the voltage generated by the "Max Voltage Switching" and "Switched Inductor". It is apparent that if SW_P is controlled as prescribed, the "Switched Inductor" offers significant improvement.

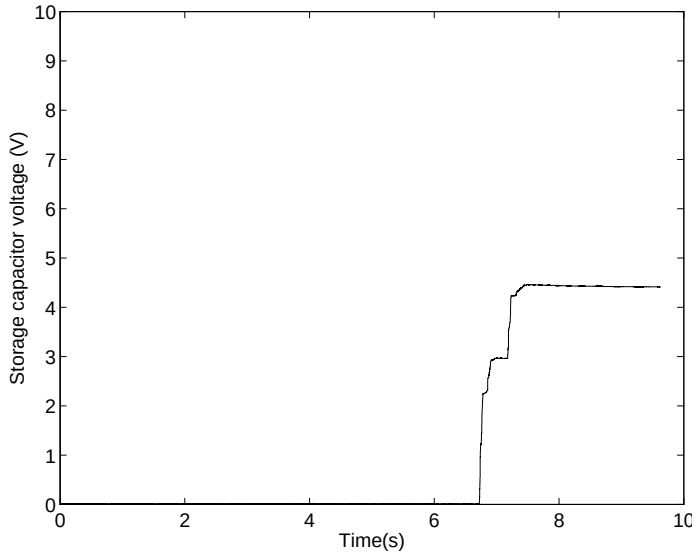

Figure 28: Max Switching

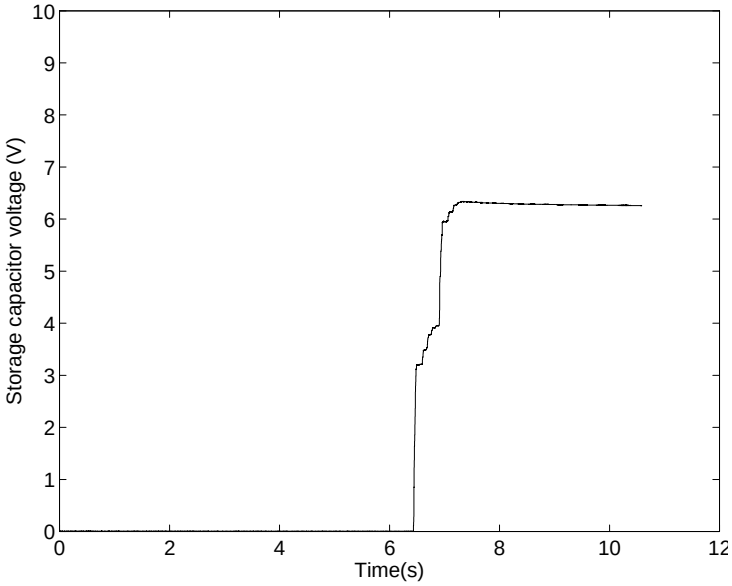

Figure 29: Switched Inductor

Figure 28 shows the influence of vehicle weight on the voltage across the storage capacitor. The figures on the left correspond to a passenger sedan while the figures on the right correspond to a motorcycle passing over the sensor. It can be clearly seen that the storage voltage for the motorcycle is smaller than the storage voltage for the car. Further results also showed that the storage voltage for a mini-van was higher than the storage voltage for the passenger sedan and reached a value as high as 7 volts. This demonstrates that the sensor is capable of roughly measuring vehicle weight. Since the transmission pulse width is proportional to the storage capacitor voltage, a rough measure of the vehicle weight can be obtained by measuring the time-width of the received wireless transmission pulse.

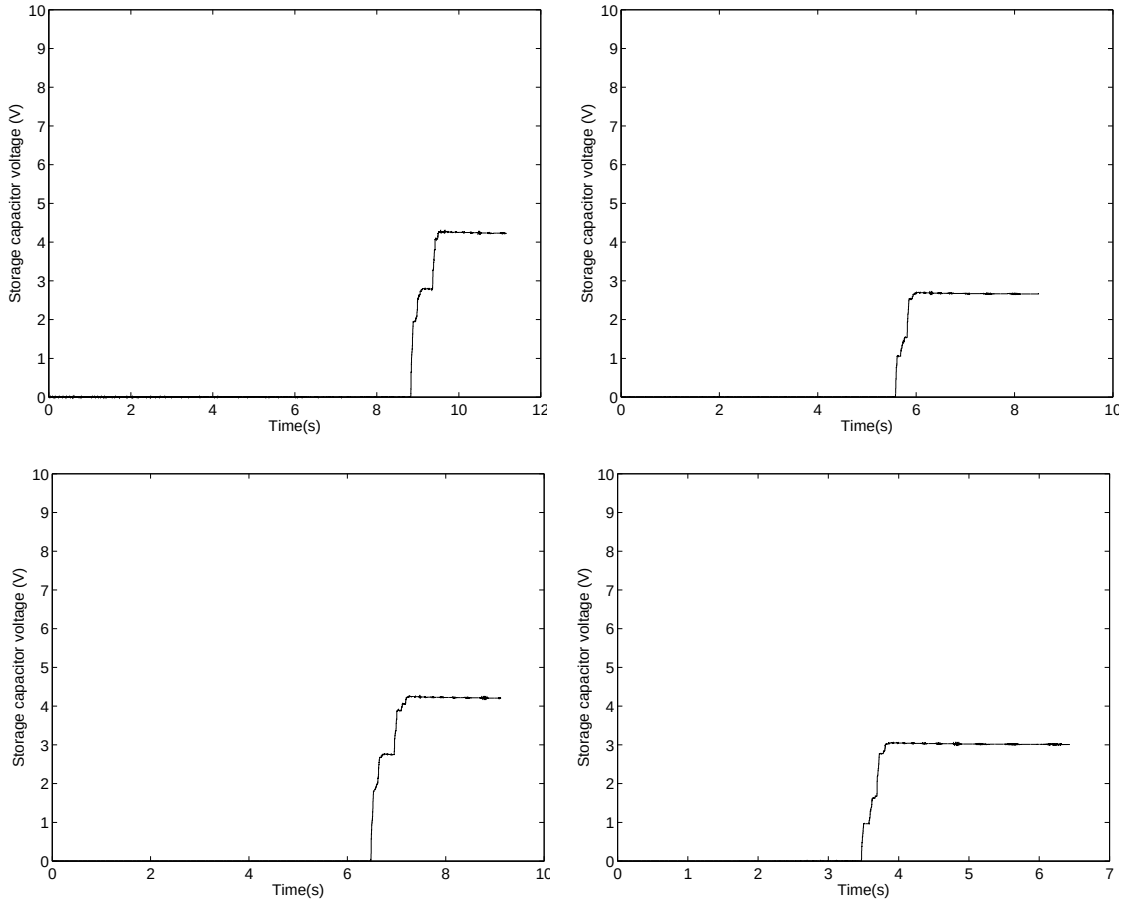

Figure 30: Capacitor Voltage Dependent on Vehicle Weight (Left: Car Driven Close to the Center @12.5 mph; Right: Motorcycle Driven Close to the Center @12.5mph)

V. TRAFFIC SENSOR NETWORKS

A. Introduction

The feasibility of a single battery-less wireless traffic sensor has been experimentally demonstrated. The current sensor will transmit an RF pulse per axle to a dedicated receiving station upon the arrival of an automobile. In the presence of multiple sensors found in sensor networks, such as at an intersection or on a highway with many lanes, the sensor should "sign" the transmission so that the receiver will be able to identify the source of transmission. This section proposes a solution for such a sensor signature.

B. Encoder Decoder

Outline

The proposed solution involves assigning a signature to each sensor in the form of a unique identification number. When a vehicle passes over the sensor, it would harvest energy from the mechanical vibrations. An encoder is used to encode this identification number to a sequence of '1's and '0's. A transmitter modulates an RF carrier wave to transmit this sequence of '1's and '0's to a receiver. Upon receiving this signal, the receiver demodulates the RF signal and recreates the series of '1's and '0's at its output. A decoder is used to convert this sequence back to the identification numbers number that was transmitted. The decoded signature is used to identify the sensor over which the automobile has passed. The schematic of the circuit to implement this scheme is shown in figure 29.

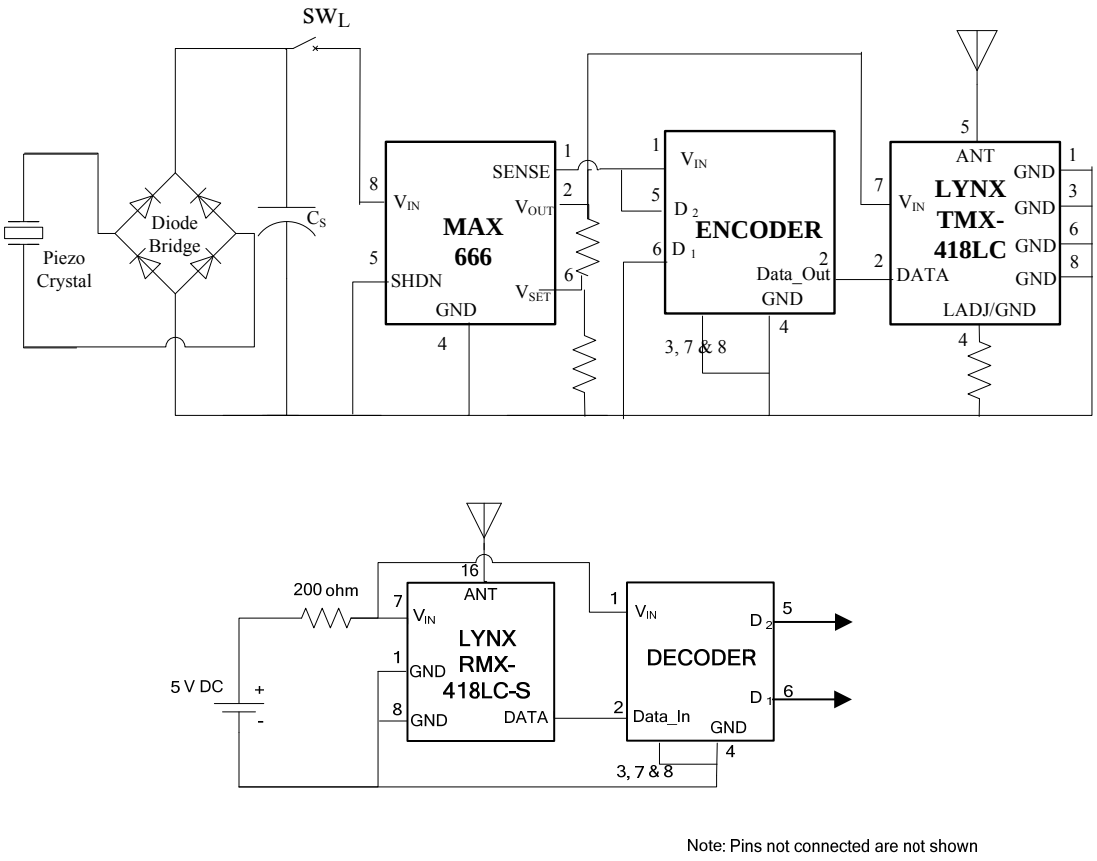

Figure 31: Circuit Schematic

Power Calculations

For the receiving station to reliably decode the transmitted signature, a minimum transmission of 20 ms is required and the supply voltage needs to be maintained at atleast 1.5V. Hence the system shall be designed to transmit for 25 ms. From our experiments, the total current required by the new circuit was calculated to be 2mA. For a 10 μF storage capacitor that is being used, this corresponds to a voltage change of 5V. Since the minimum acceptable voltage for the storage capacitor is 1.5V, enough energy must be harvested from the vibrations to charge the storage capacitor to 6.5-8V. This is expected to be possible with the switched inductor control system.

C. Experimental Results

The circuit shown in figure 29 was implemented and the traffic sensor was excited by a short duration load. For the first experiment, the encoder was configured to transmit a '1' for bit 1 (D_1) and a '0' for bit 2 (D_2). Figure 30 shows the storage capacitor voltage for the first experiment. From figure 31, showing the outputs of bit 1 (D_1) and bit 2 (D_2) of the decoder, it is seen that the sensor identification number can be successfully decoded. For the second experiment, the encoder was configured to transmit a '0' for bit 1 (D_1) and a '1' for bit 2 (D_2). Figure 32 shows the storage capacitor voltage for the first experiment. From figure 33, showing the outputs of bit

1 (D_1) and bit 2 (D_2) of the decoder, it is seen that the sensor identification number can be successfully decoded.

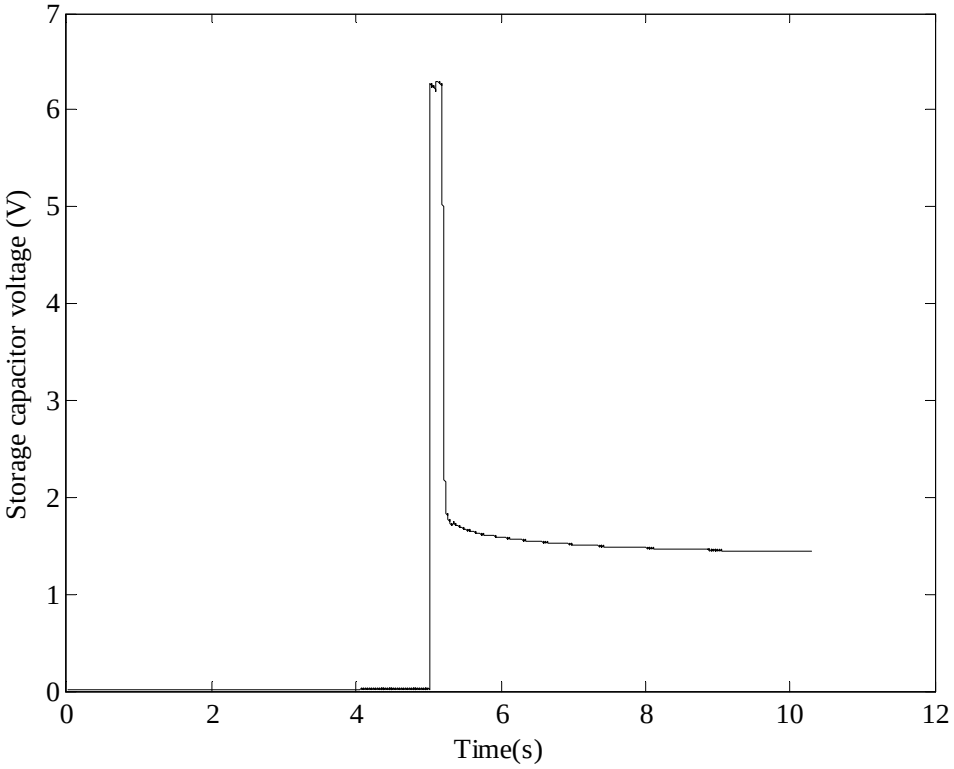

Figure 32: Storage Capacitor Voltage (1st Configuration of Encoder)

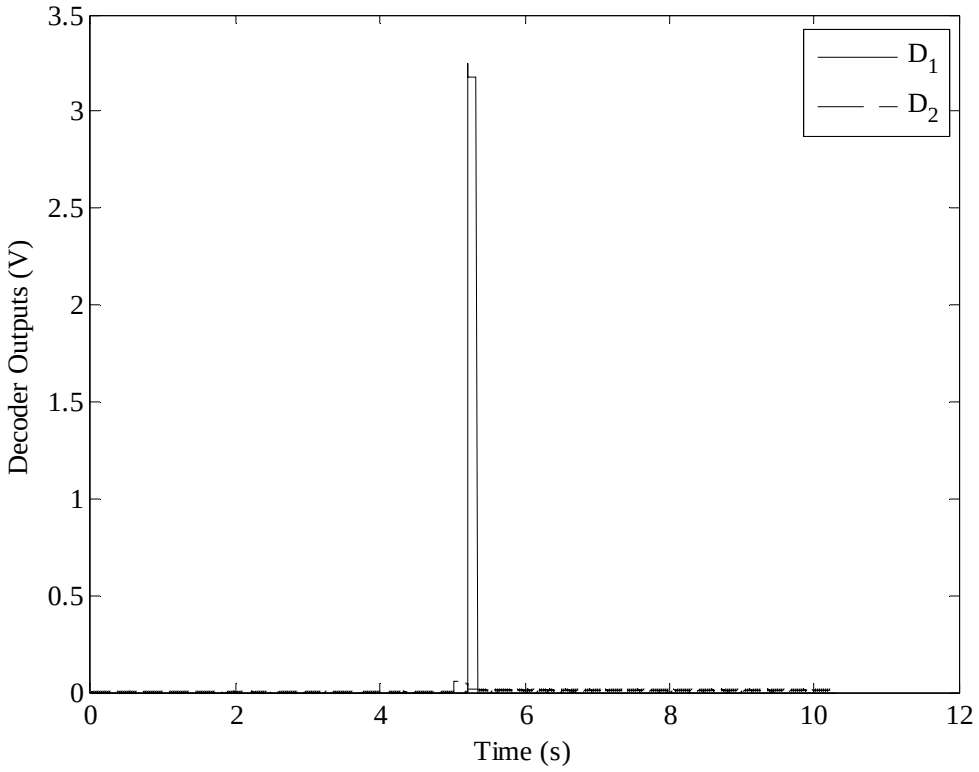

Figure 33: Decoder Output (1st Configuration of Encoder)

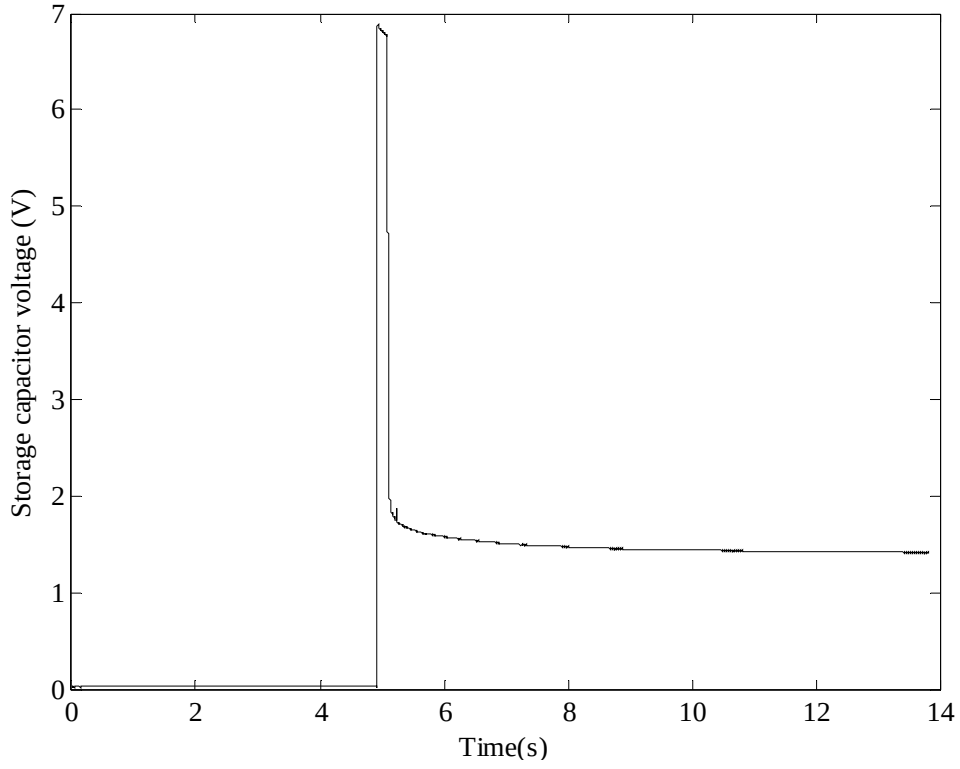

Figure 34: Storage Capacitor Voltage (2nd Configuration of Encoder)

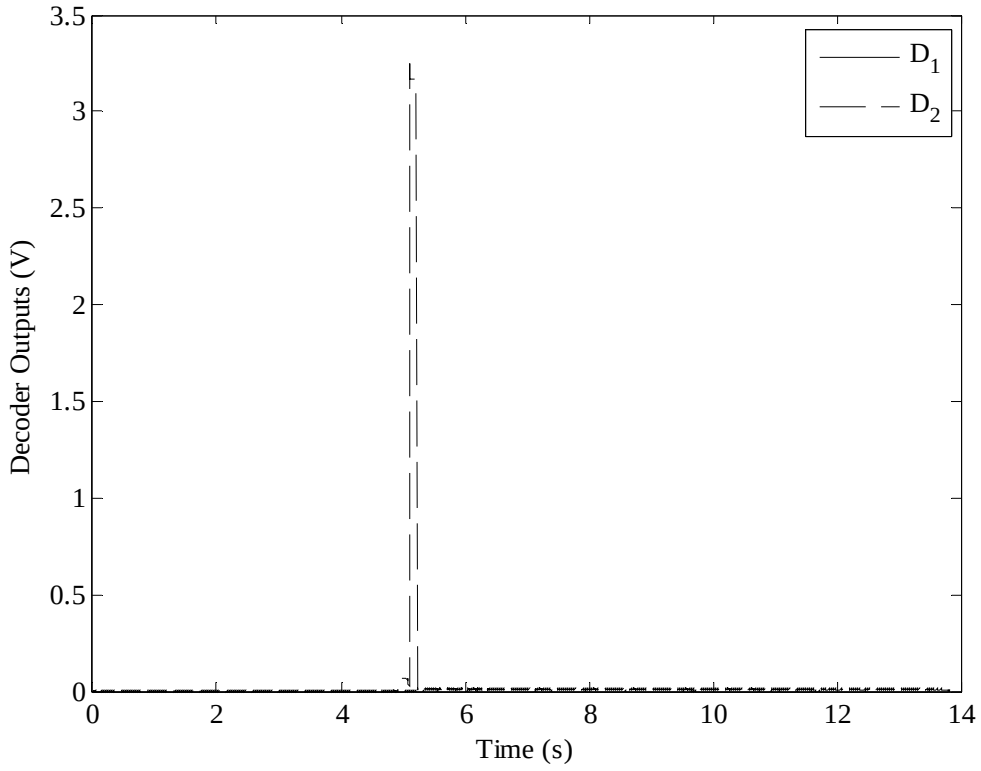

Figure 35: Decoder Output (2nd Configuration of Encoder)

VI. COMPLETION OF PROJECT TASKS

The tasks in the project that summarize the major activities which were accomplished are as follows:

1) To develop robust roadworthy electronic hardware that can be used for evaluation of all the sensors developed in this project. This will be done by fixing problems with the current data acquisition hardware, developing a new PCB that can accommodate different control systems for energy harvesting and finally by carrying out vehicle tests to verify the working of the new measurement hardware.
2) To develop and simulate key control algorithms to maximize energy harvesting from piezoelectric system. The best algorithm will then be selected and used for the remaining related tasks in this project.
3) To develop piezoelectric sensor design to enable weigh-in-motion in addition to vehicle counting, axle counting and speed measurements **(Full sensor).**
4) To evaluate the use of surface acoustic wave (SAW) devices to enable battery-less wireless operation of the roadway embedded sensors.
5) To develop piezoelectric sensor design with minimal size and optimal ease of installation to enable vehicle counting, axle counting and speed measurements **(Basic sensor)**.
6) To conduct experimental vehicle tests to evaluate performance, reliability and accuracy of full sensor.
7) To conduct experimental vehicle tests to evaluate performance, reliability and accuracy of basic sensor.
8) To develop and evaluate a sensor network in order to enable short term traffic sensor applications such as turn analysis at rural intersections. A single micro-processor capable of simultaneously receiving and analyzing signals from multiple sensors will be developed.
9) To write a comprehensive project report describing the technology developed, results obtained and conclusions reached from the work completed in the project.

All of the above tasks have been completed. The previous chapters provide details of the design, technical analysis, simulation results and experimental test data. Two important issues need to be described with respect to the list of tasks above:

A. Full Sensor Vs Basic Sensor

When the project proposal was written, the PI envisioned two different types of sensors:

1) A full sensor that would be capable of measuring traffic flow rate, number of axles on vehicle and approximate vehicle weight.
2) A basic sensor that would be capable of measuring only traffic flow rate and would be more compact and size-optimal than the full sensor.

Analysis during the project showed that the sensor must be 6 feet long in order to ensure that one set of wheels of every passing vehicle would travel over the sensor. It turned out that the wheels of the passing vehicle would have to travel directly over the sensor in order to be able to generate enough energy to power the electronics for wireless transmission. Hence the optimal sensor size

that could be obtained would be a sensor that is 6 feet long with minimal height and minimal width. This is the final size of the sensor as developed and tested in this project. While this sensor is a "basic" sensor in terms of its size optimality, it is also capable of measuring not only traffic flow rate but also approximate vehicle weight and number of axles on vehicle. Hence the distinction between a full sensor and a basic sensor could not really be made in the project. Figures 1 and 2 in this report could be considered to represent the original full sensor and basic sensor respectively. However, the basic sensor is also able to measure the approximate vehicle weight and therefore provides the same functionality as the full sensor.

B. Use of SAW Device for Battery-Less Wireless Operation

A surface acoustic wave (SAW) device was considered as an alternate method of obtaining battery-less wireless operation. SAW devices were fabricated and the interrogator electronics for interfacing with the SAW device were developed. Battery-less wireless operation with the SAW device was tested. However, it was eventually abandoned due to the fact that we could only obtain wireless telemetry distances of the order of a few feet using this technology. On the other hand, the method of harvesting energy from the sensor vibrations using piezoelectric elements and power electronics and using this energy to power a wireless transmitter was able to provide telemetry distances of over a hundred feet. Hence the clear superiority of this approach led us to abandon the surface acoustic wave approach.

VII. CONCLUSIONS

This project developed a battery-less wireless traffic sensor for measurement of traffic flow rate, number of vehicle axles and approximate vehicle weight. To the best of our knowledge, this is a unique invention and is the first ever presentation of a traffic flow sensor that obtains energy for its operation entirely by harvesting vibration energy from the passing of a vehicle over the sensor.

The developed sensor is 6 feet long, about an inch in width and 2 inches in height. It can be placed in a rectangular slot made in the roadway. This particular project focused on design of the sensor, development of control algorithms to maximize the energy harvested from the vibrations, simulation studies and experimental tests to evaluate the performance of the sensor.

Experimental results showed that the sensor was able to harvest adequate energy for its operation from the passing of every axle over the sensor. The sensor could reliably and accurately measure traffic flow rate. The width of the wireless transmission pulse from the sensor was roughly proportional to the weight of the vehicle passing over the sensor. Thus the vehicle weight could also be approximately measured.

Compared to existing inductive loop detectors, the developed new sensors have the following advantages:

1) **Installation:** To install a loop detector and calibrate it, it is sometimes necessary to shut down traffic on the road for as much as 2 days. The new sensors can be installed by drilling a slot across the lane in the road surface of 1 inch width and 2 inches depth. Most importantly, no wiring is needed from the traffic lane to the roadside data acquisition unit. It is expected that the installation will only take a few minutes.
2) **Energy consumption:** The sensors on the roadway require no external power supply while inductive loop detectors have to be continuously powered all the time, even during the night when traffic flow might be really low.
3) **Cost:** A 4-channel loop detector package (for example, from Eberle Design, Inc or Reno A&E) on average has a hardware cost of around $700. The *installed* cost of each loop is typically around $1500. The proposed sensors on the other hand are expected to cost only $50 - $100 each.
4) **Additional Variables:** The new sensors can measure number of axles and vehicle length, in addition to traffic flow rate. Thus they can be used for vehicle classification. With some further development, the sensors can likely also be used for weigh-in-motion.

Future work will focus on further enhancing the telemetry distance of the sensor so that it can directly transmit wireless readings to a central metro location, improving the weigh-in-motion ability of the sensor and field testing of the sensor by placing it in a pavement location where it can be repeatedly tested with known traffic flow rates and known vehicle loads.

REFERENCES

[1] C. Chen, J. Kwon, J. Rice, A. Skabardonis and P. Varaiya, "Detecting errors and imputing missing data for single-loop surveillance systems," *Transportation Research Record*, pp.160-167, 2003.

[2] S. Chen, Z. Sun and B. Bridge, "Traffic Monitoring Using Digital Sound Field Mapping", *IEEE Transactions on Vehicular Technology*, vol. 50, no. 6, pp.1582-1589, 2001.

[3] S. Chen, Z. P. Sun and B. Bridge, "Automatic traffic monitoring by intelligent sound detection", *IEEE Conference on Intelligent Transportation Systems*, pp.171-176, 1997.

[4] B. Coifman, "Improved Velocity Estimation Using Single Loop Detectors", *Transportation Research Part A: Policy and Practice*, vol. 35, no. 10, pp.863-880, 2001.

[5] C. W. De Silva, *Mechatronics: An Integrated Approach*, CRC Press, 2004.

[6] N. Ferrier, S. Rowe and A. Blake, "Real-time traffic monitoring", *Proceedings of the Second IEEE Workshop on Applications of Computer Vision*, pp.81-88, 1994.

[7] W. E. L. Grimson, C. Stauffer, R. Romano and L. Lee, "Using adaptive tracking to classify and monitor activities in a site," *Proceedings of the IEEE Computer Society Conference on Vision and Pattern Recognition*, pp.22-29, 1998.

[8] P. Horowitz and W. Hill, *The Art of Electronics*, Cambridge University Press, 1989.

[9] S. Kamijo, Y. Matsushita, K. Ikeuchi and M. Sakauchi, "Traffic monitoring and accident detection at intersections", IEEE Transactions on Intelligent Transportation Systems, vol. 1, no. 2, pp.108-118, 2000.

[10] H. K. Khalil, *Nonlinear Systems*, Upper Saddle River, New Jersey, Prentice Hall, 2002.

[11] S. W. Kim, Y. Eun, H. Kim, J. Ko, W. J. Jung, Y. Choi, Y. G. Cho and D. Cho, "Performance comparison of loop/piezo and ultrasonic sensor-based traffic detection systems for collecting individual vehicle information", *Proceedings of the 6th World Congress on ITS* (CD-ROM), 1998.

[12] S. W. Kim, K. Kim, J. Lee and D. D. Cho, "Application Of Fuzzy Logic to Vehicle Classification Algorithm In Loop/Piezo-Sensor Fusion Systems", *Asian Journal of Control*, vol. 3, no. 1, pp.64-68, 2001.

[13] P. V. Kokotovic, J. O'Reilly and H. K. Khalil, *Singular Perturbation Methods in Control: Analysis and Design*, Society for Industrial and Applied Mathematics, Philadelphia, 1986.

[14] C. Li, K. Ikeuchi and M. Sakauchi, "Acquisition of Traffic Information Using Video Camera with 2D Spatio-Temporal Image Transformation Technique", *IEEE Transactions on Intelligent Transportation*, pp.634-638, 1999.

[15] E. Lefeuvre, A. Badel, C. Richard, D. Guyomar, "Piezoelectric Energy Harvesting Device Optimization by Synchronous Electric Charge Extraction," *Journal of Intelligent Materials, Systems and Structures*, vol. 16, no. 10, pp.865-876, 2005.

[16] L.J. Mountain, J. B. Garner. , "Application of photography to traffic surveys", *The Journal of the Institute of Highway Engineers*, pp.12-19, 1980.

[17] P. T. Martin, Y. Feng and X. Wang, *Detector Technology Evaluation*, Mountain-Plains Consortium, 2003.

[18] P. G. Michalopoulos and C. A. Anderson, "Costs and benefits of vision-based, wide-area detection in freeway applications," *Transportation Research Record*, pp.40-47, 1995.

[19] O. D. Nwokah, *Mechanical Systems Design Handbook Modeling Measurement and Control*, CRC Press, 2001.

[20] S. Oh, S. G. Ritchie and C. Oh "Real Time Traffic Measurement from Single Loop Inductive Signatures," 81st *TRB Annual Meeting*, January 2002.
[21] G. K. Ottman, H. F. Hofmann, A. C. Bhatt and G. A. Lesieutre. , "Adaptive piezoelectric energy harvesting circuit for wireless remote power supply," *IEEE Transactions on Power Electronics*, vol. 17, no. 5, pp.669-676, 2002.
[22] J. C. Rojas and J. D. Crisman. , "Vehicle detection in color images", *Intelligent Transportation System*s, IEEE Conference on ITS, pp.403-408, 1997.
[23] Santiram Kal, *Basic Electronics: Devices, Circuits and IT Fundamentals*, Prentice Hall of India, 2004.
[24] H. A. Sodano, D. J. Inman and G. Park. , "Comparison of Piezoelectric Energy Harvesting Devices for Recharging Batteries", *Journal of Intelligent Materials, Systems and Structures*, vol. 16, no. 10, pp.799-807, 2005.
[25] H. A. Sodano, D. J. Inman and G. Park, "A Review of Power Harvesting from Vibration Using Piezoelectric Materials", *The Shock and Vibration Digest*, vol. 36, no. 3, pp.197-205, 2004.
[26] C. Sun, S. G. Ritchie and S. Oh, "Inductive Classifying Artificial Network for Vehicle Type Categorization", *Computer-Aided Civil and Infrastructure Engineering*, vol. 18, no. 3, pp.161-172, 2003.
[27] Urban ITS Center at Polytechnic University, "User's Manual For Cost Estimates of Intelligent Transportation Technologies (CEIT)," Under sub-contract with Calspan University at Buffalo Research Center, 2001.
[28] N. Ushio and T. Shimizu, "Loop vs ultrasonic in Chicago: Ultrasonic vehicle detector field test isolating diffused reflection and enduring harsh environment", Proceedings of the 5th World Congress on Intelligent Transportation Systems, Seoul, Korea, 1998.
[29] M. A. Vicencio, B. Qiu and M. G. Hartley, "Algorithms and architectures for the analysis of road-trafficmovements", Third International Conference on Image Processing and its Applications, University of Warwick, pp.182-186, 1989.
[30] M.S. Weinberg, "Working equations for piezoelectric actuators and sensors", *Journal of Microelectromechanical Systems*, vol. 8, no. 4, pp.529-533, 1999.